A Time-Domain Green's Function for Interaction between Water Waves and Floating Bodies with Viscous Dissipation Effects

Zhiqun Guo [1], Q. W. Ma [1,2] and Hongde Qin [1,*]

[1]   College of Shipbuilding Engineering, Harbin Engineering University, Harbin 150001, China;
       guozhiqun@hrbeu.edu.cn (Z.G.); Q.Ma@city.ac.uk (Q.W.M.)
[2]   School of Engineering and Mathematical, City University London, London EC1V 0HB, UK
[*]   Correspondence: qinhd@hrbeu.edu.cn; Tel.: +86-137-0451-3212

Abstract: A novel time-domain Green's function is developed for dealing with two-dimensional interaction between water waves and floating bodies with considering viscous dissipation effects based on the "fairly perfect fluid" model. In the Green's function, the temporal (lower order viscosity coefficient term) and spatial (higher order viscosity coefficient term) viscous dissipation effects are fully considered. As compared to the methods based on the existing time-domain Green's functions that could not account for the spatial viscous dissipation, the method based on the new time-domain Green's function can give much better numerical results and overcome instability problems related to the existing Green's function, according to the numerical tests and comparison with CFD modeling data for a few cases related to floating bodies with a flare angle.

Keywords: water waves; Green's function; viscous dissipation effects; interaction between water waves and floating bodies

1. Introduction

The interaction between water waves and floating bodies is one of most common occurrences in marine or ocean engineering. The interaction could induce ships or floating platforms to make six degree of freedom (6-DOF) motions, and wave loads may bring damage for the structures. Therefore, it is of great significance to investigate the interaction between water waves and floating bodies. There are many numerical methods that could be employed for such purpose, such as Green's function methods, finite element methods, meshless methods and so on. Among these methods, Green's function methods are most efficient because they are linear panel methods with panels or segments distributed only on the wetted surface of floating bodies.

As a result of ignoring fluid viscosity, the conventional inviscid Green's function methods encounter difficulties in solving some water surface hydrodynamic problems associated with viscosity, such as the decay of gravity waves during propagating and exact amplitude of resonant waves in shielded waters. To overcome those, two main viscous correction models are proposed in the literature to improve the Green's function methods. In these two models, Green's functions are obtained by solving boundary value problems with viscous correction (BVP_V), in which the free-surface conditions are corrected by a viscous dissipation term, while other conditions remain the same as the inviscid ones.

The first model is based on the "fairly perfect fluid" [1], where the dissipation term in the linear momentum equation is $-v\nabla\psi$ ($v \geq 0$ is an artificial viscosity coefficient). In this model, the linear

Bernoulli's equation and free-surface condition with viscous dissipation term can be, respectively, written as [1,2]

$$
\begin{cases}
\frac{\partial \psi}{\partial t} + \frac{p}{\rho} + g\eta + \upsilon\psi = 0 \\
\frac{\partial^2 \psi}{\partial t^2} + g\frac{\partial \psi}{\partial y} + \upsilon\frac{\partial \psi}{\partial t} = 0
\end{cases}
\tag{1}
$$

The second model is based on the linear incompressible NS equations, from which the linear Bernoulli's equation and free-surface condition can be, respectively, deduced as follows [3,4]

$$
\begin{cases}
\frac{\partial \psi}{\partial t} + \frac{p}{\rho} + g\eta + 2\nu\frac{\partial^2 \psi}{\partial y^2} = 0 \\
\frac{\partial^2 \psi}{\partial t^2} + g\frac{\partial \psi}{\partial y} + 4\nu\frac{\partial^3 \psi}{\partial t \partial y^2} = 0
\end{cases}
\tag{2}
$$

where oy axis points upward; and ν and ψ are physical kinematic viscosity coefficient and velocity potential of the fluid, respectively.

For the sake of distinction, in this paper, the Green's function derived using the first and second models are called the first and second kind of Green's function with viscous dissipation effects (GF_1_V and GF_2_V), respectively. Although the viscous dissipation term in Equation (1) is simpler than that in Equation (2), it was indicated [4] that the two viscous correction approaches are equivalent to each other due to the relationship between the artificial viscosity coefficient υ and the physical kinematic viscosity coefficient ν: $\upsilon = 4\nu k^2$, where k is the wave number.

Although the viscous dissipation term in Equations (1) or (2) is linear with respect to the viscosity coefficient, the exact Green's function with viscous dissipation effects (GF_V) derived from the BVP_V is nonlinear to it. Nonetheless, nearly all GF_V proposed in the literature only exactly contain the lower order viscosity coefficient term, while the higher order ones are not fully considered. Admittedly, the GF_V with lower order viscosity coefficient term (GF_V_1) are sufficient to solve general water wave problems, since in these problems the viscosity coefficients are low enough (the same as or analog to real viscosity of water) to make the high order viscosity coefficient terms insignificant. The major works in this respect are enumerated as follows. Chen [2] first proposed a GF_1_V_1 to eliminate the numerical resonance phenomena in multi-body hydrodynamics, and a similar work was followed [5]. Then, a GF_2_V_1 was developed to analyze the time-harmonic ship waves [4]. Further, a tank GF_2_V_1 was presented for investigating the realistic effects of water viscosity and side walls on waves in tanks [6].

The GF_V_1, however, should not be appropriate for solving the hydrodynamic problems associated with larger fluid viscosity (e.g., the sloshing of oil in the cargo tank) or with vortex shedding around sharp edges of floating bodies, the later of which accompanies with significant fluid pressure and flow energy loss. This is because the viscous dissipation effects in such cases are so large that the higher order viscosity coefficient terms in GF_V cannot be ignored. Nevertheless, several attempts of applying GF_V_1 on solving such problems were also made in some works. Chen et al. [7] set a dissipation surface from the sharp edge of a moonpool down to the seabed, imposed a continuous flow velocity but a discontinuous pressure across this dissipation surface to simulate the pressure loss near the sharp edge, and then employed a GF_1_V_1 to solve the BVP_V. Analogously, Cummins and Dias [8] proposed a pressure discharge model to evaluate the viscous dissipation effects near a flap's edge. One should notice that in these two works the GF_V_1 was not used alone but in combination with additional pressure correction models in the vicinity of sharp edges.

All abovementioned GF_V are in frequency-domain, which are only suitable for solving steady BVP_V. To investigate general initial BVP_V, the time-domain Green's functions with viscous dissipation effects (TGF_V) are required. However, very few efforts have been carried out in this respect. A representative work was performed by Wu [9], who developed a three-dimensional (3D) TGF_2_V_1. The main goal of Wu's work was to eliminate the numerical instability of the TGF using the viscous dissipation effects, because the conventional TGF suffer numerical instability in solving hydrodynamics of floating bodies with flare angles [10]. However, Wu's attempt failed when he utilized the TGF_2_V_1

with the physical viscosity of water to study a cone heaving on the water surface. Wu's failure mainly results from the weak viscosity of water and without consideration of higher order viscosity coefficient terms in $TGF_2\_V_1$. Similar to the vortex shedding cases, one should artificially enlarge the viscosity coefficient in TGF_V, as well as take the high order viscosity coefficient terms into account to enhance the numerical stability of the TGF method.

From the above, it is clear that existing GF_V only contain the first order viscosity coefficient term, and were mainly applied to solve the viscous water wave problems, while the problems associated with vortex shedding or numerical instability in time-domain were not well addressed. Moreover, GF_V with higher order viscosity coefficient terms have not been investigated.

In this paper, a novel TGF_1_V with exact viscosity coefficient terms ($TGF_1\_V_\infty$) is developed in strict accordance with the corresponding BVP_V. One will witness later that $TGF_1\_V_\infty$ not only includes the higher order viscous dissipation effects in the free surface memory term of TGF_V_1, but also completely modifies the instantaneous term of $TGF_1\_V_1$ or TGF_1. Without loss of generality, the proposed $TGF_1\_V_\infty$ are limited to the two-dimensional (2D) flows with infinite depth, which have never been studied in literature. In fact, the 2D TGF_V are able to evaluate the viscous dissipation effects on hydrodynamics not only of 2D zero-speed floating bodies, but also of 3D high-speed ships within the 2.5D or 2D + *t* framework [11]. Moreover, the approach provided here for developing the 2D $TGF_1\_V_\infty$ can also be employed for developing other types of GF_V_∞.

The newly proposed (2D) $TGF_1\_V_\infty$ are employed to improve the numerical stability of a wedge heaving on the water surface, and then to evaluate the added mass and damping of a hull section with sharp keel rolling on the water surface, in which vortex shedding occurs. The object of the present paper is to shed light on the intrinsic characteristic of the $TGF_1\_V_\infty$, and to extend the application of GF_V or TGF_V on interaction between water waves and floating bodies with viscous dissipation effects rather than the viscous surface wave problems.

2. Mathematical Models of $TGF_1\_V_\infty$

Let TGF_1_V be the first kind of time-domain Green's function with viscous dissipation effects that derived by solving the BVP with free-surface condition in Equation (1). Let $TGF_1\_V_n$ be a TGF_1_V that exactly contains first *n* orders viscosity coefficient terms, and $TGF_1\_V_\infty$ be the TGF_1_V that exactly satisfies the definite conditions of the BVP_V. In this section, the mathematical model of $TGF_1\_V_\infty$ is derived. For the purpose of comparison, the model of $TGF_1\_V_1$ is also given.

2.1. Definite Problem for $TGF_1\_V_n$

A right-hand Cartesian coordinate system $o-xy$ is defined by placing ox axis on the undisturbed water surface and the oy axis oriented positively upward. Let $G_{1\_n}(\boldsymbol{p},t;\boldsymbol{q},\tau;\epsilon)$ be the expression of $TGF_1\_V_n$ representing the velocity potential at a field point $\boldsymbol{p}(x,y)$ at time *t* in the 2D fluid domain Ω with non-dimensional viscosity coefficient ϵ due to a pulsating source of unit strength at the point $\boldsymbol{q}(\xi,\eta)$ at time τ. $G_{1\_n}(\boldsymbol{p},t;\boldsymbol{q},\tau;\epsilon)$ can be expressed as the combination of instantaneous term $\overline{G}_{1\_n}(\boldsymbol{p},\boldsymbol{q};\epsilon)$ and free-surface memory term $\widetilde{G}_{1\_n}(\boldsymbol{p},t;\boldsymbol{q},\tau;\epsilon)$

$$G_{1\_n}(\boldsymbol{p},t;\boldsymbol{q},\tau;\epsilon) = \delta(t-\tau)\overline{G}_{1\_n}(\boldsymbol{p},\boldsymbol{q};\epsilon) - H(t-\tau)\widetilde{G}_{1\_n}(\boldsymbol{p},t;\boldsymbol{q},\tau;\epsilon) \tag{3}$$

where the non-dimensional viscosity coefficient ϵ is defined as $\epsilon = v/2\omega_0$, $\delta(\cdot)$ is Dirac function, $H(\cdot)$ is Heaviside function, and ω_0 is the reference frequency. Both instantaneous term $\overline{G}_{1\_n}(\boldsymbol{p},\boldsymbol{q};\epsilon)$ and free-surface memory term $\widetilde{G}_{1\_n}(\boldsymbol{p},t;\boldsymbol{q},\tau;\epsilon)$ in Equation (3) may contain viscous dissipation effects

and differ from the inviscid ones. When the non-dimensional viscosity coefficient ϵ approaches zero, $\text{TGF}_1\_V_n$ should approach to the inviscid TGF

$$
\begin{aligned}
G(\boldsymbol{p},t;\boldsymbol{q},\tau) &= \delta(t-\tau)\,\overline{G}(\boldsymbol{p},\boldsymbol{q}) - H(t-\tau)\widetilde{G}(\boldsymbol{p},t;\boldsymbol{q},\tau) \\
&= \delta(t-\tau)\ln\frac{r_{pq}}{r_{p\bar{q}}} - H(t-\tau) \\
&\quad \times 2\int_0^\infty \sqrt{\frac{g}{k}}e^{k(y+\eta)}\cos(k(x-\xi))\sin\left(\sqrt{gk}(t-\tau)\right)\mathrm{d}k
\end{aligned}
\tag{4}
$$

where r_{pq} and $r_{p\bar{q}}$ are the distance from field point $\boldsymbol{p}$ to source point $\boldsymbol{q}$ and $\bar{\boldsymbol{q}}$ (mirror point of $\boldsymbol{q}$ with respect to the water surface), respectively.

Taking Equations (1) and (2) into account, the free-surface memory term $\widetilde{G}_{1\_n}(\boldsymbol{p},t;\boldsymbol{q},\tau;\epsilon)$ satisfies the following definite conditions

$$
\begin{cases}
\nabla_q^2 \widetilde{G}_{1\_n} = 0, & \boldsymbol{p},\boldsymbol{q}\in\Omega, t>\tau \\
\frac{\partial^2 \widetilde{G}_{1\_n}}{\partial\tau^2} + g\frac{\partial \widetilde{G}_{1\_n}}{\partial\eta} - 2\epsilon\omega_0\frac{\partial \widetilde{G}_{1\_n}}{\partial\tau} = 0, & \eta = 0 \\
\widetilde{G}_{1\_n} = 0, & t = \tau \\
\nabla_q \widetilde{G}_{1\_n} = 0, & r_{pq}, r_{p\bar{q}} \to \infty \\
\widetilde{G}_{1\_n} = \widetilde{G}, & \epsilon \to 0
\end{cases}
\tag{5}
$$

where the subscript q from ∇_q, ∇_q^2 means that the operation is taken with respect to variant $\boldsymbol{q}$. In the second part of Equation (5), the sign of the viscous term changes to minus due to the relation $\partial \widetilde{G}_{1\_n}/\partial\tau = -\partial \widetilde{G}_{1\_n}/\partial t$.

One should note that definite conditions for $\overline{G}_{1\_n}$ are not independent to $\widetilde{G}_{1\_n}$, instead they should be derived through the boundary integral equation, which connects $\overline{G}_{1\_n}$ and $\widetilde{G}_{1\_n}$ with each other.

2.2. Free-Surface Memory Term of $\text{TGF}_1\_V_n$

Applying the Fourier transform to the governing equations (Equation (5)) and taking initial and boundary value conditions into account, the following free-surface memory terms are obtained

$$
\widetilde{G}_{1\_\infty} = 2\int_0^\infty \sqrt{\frac{g}{k}}e^{(k+\epsilon^2 k_0)(y+\eta)}e^{-\epsilon\omega_0(t-\tau)}\cos\left(\left(k+\epsilon^2 k_0\right)(x-\xi)\right)\sin\left(\sqrt{gk}(t-\tau)\right)\mathrm{d}k
\tag{6}
$$

where $k_0 = \omega_0^2/g$ is the reference wave number.

From Equation (6) we can write the $\widetilde{G}_{1\_1}$ as

$$
\widetilde{G}_{1\_1} = 2e^{-\epsilon\omega_0(t-\tau)}\int_0^\infty \sqrt{\frac{g}{k}}e^{k(y+\eta)}\cos(k(x-\xi))\sin\left(\sqrt{gk}(t-\tau)\right)\mathrm{d}k
\tag{7}
$$

The free-surface memory terms $\widetilde{G}_{1\_n}$ given in Equations (6) and (7) for 2D $\text{TGF}_1\_V_n$ are new. As comparison, Wu [9] only gave the $\widetilde{G}_{2\_1}$ for 3D $\text{TGF}_2\_V_1$, in which the first order viscosity coefficient term is $e^{-\nu k^2(t-\tau)}$, equivalent to $e^{-\epsilon\omega_0(t-\tau)}$ in (7).

Rewriting Equations (6) and (7) by complex expressions, one gets

$$
\widetilde{G}_{1\_n} = \mathrm{Re}\left\{\mu_{1\_n}(\epsilon)\times 2\int_0^\infty \sqrt{\frac{g}{k}}e^{k(y+\eta+\mathrm{i}(x-\xi))}\sin\left(\sqrt{gk}(t-\tau)\right)\mathrm{d}k\right\}
\tag{8}
$$

where $\mathrm{Re}\{\cdot\}$ is the real part of the complex number, and $\mu_{1\_n}(\epsilon)$ the viscous dissipation effects term defined as

$$
\mu_{1\_n}(\epsilon) = \begin{cases}
e^{-\epsilon\omega_0(t-\tau)}, & n = 1 \\
e^{-\epsilon\omega_0(t-\tau)}e^{\epsilon^2 k_0(y+\eta+\mathrm{i}(x-\xi))}, & n = \infty
\end{cases}
$$

In contrast, the inviscid free-surface memory term in Equation (4) can be written as

$$\widetilde{G} = \text{Re}\left\{ 2 \int_0^\infty \sqrt{\frac{g}{k}} e^{k(y+\eta+\text{i}(x-\xi))} \sin\left(\sqrt{gk}(t-\tau)\right) dk \right\} \tag{9}$$

Comparing Equation (8) with Equation (9), it clearly shows that the viscous dissipation effects in $\widetilde{G}_{1\_\infty}$ are reflected in the following aspects. The first is the time dissipation effect $e^{-\epsilon\omega_0(t-\tau)}$, which makes the disturb from the source point to the field point exponentially decay along with time. The second is the spatial dissipation effect $e^{\epsilon^2 k_0(y+\eta+\text{i}(x-\xi))}$, which accelerates the decay rate of the disturb along the depth increasing direction, as well as shifts the phase of disturb along the horizontal direction. In contrast, in the 3D $\widetilde{G}_{2\_1}$ [9] or 2D $\widetilde{G}_{1\_1}$, there only exists a lower order time dissipation term, while the higher order spatial dissipation effects are not considered.

2.3. Instantaneous Term of TGF$_1$_V$_n$

2.3.1. Definite Conditions for the Instantaneous Term of TGF$_1$_V$_n$

As stated in Section 2.1, the definite conditions for the instantaneous term $\overline{G}_{1\_n}$ are relevant to the free-surface memory term $\widetilde{G}_{1\_n}$ through the boundary integral equation. The derivation of definite conditions for $\overline{G}_{1\_n}$ is detailed in Appendix A, and the final results are as follows

$$\begin{cases} \nabla_q^2 \overline{G}_{1\_n} = \beta\delta(p-q), & p, q \in \Omega \\ \overline{G}_{1\_n} = 0, & \eta = 0 \\ \overline{G}_{1\_n} \sim O\left(\frac{1}{r_{pq}}\right), & r_{pq}, r_{p\bar{q}} \to \infty \\ \overline{G}_{1\_n} = \overline{G}, & \epsilon \to 0 \\ \frac{\partial \overline{G}_{1\_n}}{\partial \eta} = -\frac{1}{g}\frac{\partial \widetilde{G}_{1\_n}}{\partial \tau}, & t = \tau, \eta = 0 \end{cases} \tag{10}$$

where β is an unknown constant dependent on the instantaneous term $\overline{G}_{1\_n}$. One can also observe that in Equations (10) the first three conditions for $\overline{G}_{m\_n}$ are the same as the inviscid ones, while the last condition is different corresponding to different free surface memory term $\widetilde{G}_{1\_n}$.

2.3.2. Instantaneous Term of **TGF$_1$_V$_1$**

Obviously for $n = 1$ we have

$$\left.\frac{\partial \overline{G}_{1\_1}}{\partial \eta}\right|_{t=\tau,\eta=0} = 2 \int_0^\infty e^{ky} \cos k(x-\xi) dk \tag{11}$$

which is the same as the inviscid condition. Thereby, all conditions for $\overline{G}_{1\_1}$ are the same as the inviscid ones, which suggests that the expression of $\overline{G}_{1\_1}$ should be the same as the inviscid instantaneous term $\overline{G}$

$$\overline{G}_{1\_1} = \overline{G} = \ln\frac{r_{pq}}{r_{p\bar{q}}} \tag{12}$$

In [9], the 3D inviscid instantaneous term is $\overline{G}_{2\_1} = 1/r_{pq} - 1/r_{p\bar{q}}$, which is also the same as the inviscid one.

2.3.3. Instantaneous Term of TGF$_1$_V$_\infty$

One can verify that, however, the last condition in Equation (10) for $\overline{G}_{1\_\infty}$ is not the same as the inviscid one given in Equation (11). Thus, we need to design an appropriate $\overline{G}_{1\_\infty}(p, q; \epsilon)$ that satisfy all conditions in Equations (10).

Substituting Equation (6) into the last part of Equation (10) yields

$$
\begin{aligned}
\left.\frac{\partial \overline{G}_{1\_\infty}(p,q;\epsilon)}{\partial \eta}\right|_{\eta=0} &= \left.\mathrm{Re}\left\{-2\frac{e^{\epsilon^2 k_0(y+\eta+\mathrm{i}(x-\xi))}}{y+\eta+\mathrm{i}(x-\xi)}\right\}\right|_{\eta=0} \\
&\overset{*}{=} \left.\mathrm{Re}\left\{-\frac{e^{\epsilon^2 k_0(y+\eta+\mathrm{i}(x-\xi))}}{y+\eta+\mathrm{i}(x-\xi)} - \frac{e^{\epsilon^2 k_0(-|y-\eta|+\mathrm{i}(x-\xi))}}{-|y-\eta|+\mathrm{i}(x-\xi)}\right\}\right|_{\eta=0} \\
&= \left.\mathrm{Re}\left\{-\frac{e^{\epsilon^2 k_0 R_{p\bar{q}}}}{R_{p\bar{q}}} - \frac{e^{\epsilon^2 k_0 R_{pq}}}{R_{pq}}\right\}\right|_{\eta=0} \\
&= \left.\frac{\partial}{\partial \eta}\mathrm{Re}\left\{E_1\left(-\epsilon^2 k_0 R_{p\bar{q}}\right) - E_1\left(-\epsilon^2 k_0 R_{pq}\right)\right\}\right|_{\eta=0}
\end{aligned}
\tag{13}
$$

with

$$
\begin{cases}
R_{p\bar{q}} = y + \eta + \mathrm{i}(x-\xi) \\
R_{pq} = -|y-\eta| + \mathrm{i}(x-\xi)
\end{cases}
$$

$$
E_1(z) = \int_z^\infty \frac{e^{-r}}{r}\mathrm{d}r,\ z \neq 0
$$

where $E_1(z)$ is the complex exponential integral function.

In step $*$ of Equation (13), a pair of vectors $R_{p\bar{q}}$ and R_{pq} is constructed in the complex plane. The vector $R_{p\bar{q}}$ (from the mirror point $\bar{q}$ to the field point p) is straightforwardly obtained from the original equation, while the vector R_{pq} is defined as $-|y-\eta| + \mathrm{i}(x-\xi)$, which has the same value to $y + \eta + \mathrm{i}(x-\xi)$ at $\eta = 0$, rather than other forms to ensure the convergency of the numerator $e^{\epsilon^2 k_0 R_{pq}}$ in the equation. Obviously, the modulus of vectors $R_{p\bar{q}}$ and R_{pq} equals to the distance between source points and the field point, i.e., $|R_{p\bar{q}}| = r_{p\bar{q}}$, $|R_{pq}| = r_{pq}$. Then integrating the equation with respect to η, we finally obtain a possible solution $\mathrm{Re}\left\{E_1\left(-\epsilon^2 k_0 R_{p\bar{q}}\right) - E_1\left(-\epsilon^2 k_0 R_{pq}\right)\right\}$ for the instantaneous term.

It can be verified that $\mathrm{Re}\left\{E_1\left(-\epsilon^2 k_0 R_{p\bar{q}}\right) - E_1\left(-\epsilon^2 k_0 R_{pq}\right)\right\}$ satisfies all conditions in Equation (10), so we can define the instantaneous term $\overline{G}_{1\_\infty}$ as

$$
\overline{G}_{1\_\infty}(p,q;\epsilon) \equiv \mathrm{Re}\left\{E_1\left(-\epsilon^2 k_0 R_{p\bar{q}}\right) - E_1\left(-\epsilon^2 k_0 R_{pq}\right)\right\}
\tag{14}
$$

One can find that the instantaneous term $\overline{G}_{1\_\infty}$ in Equation (14) contain instantaneous spatial viscous dissipation effects, which are completely new and different from the inviscid instantaneous term $\overline{G}_{1\_1}$ or $\overline{G}$ in Equation (12). In fact, all existing GF_V in the literature including 3D TGF_V [9] do not contain spatial viscous dissipation effect, i.e., their Rankine part or instantaneous term is the same as the inviscid ones.

From the above, we know when the spatial viscous dissipation effects (higher order viscosity coefficient term) is not considered in the free-surface memory term ($\widetilde{G}_{1\_1}$), the instantaneous term $\overline{G}_{1\_1}$ for TGF$_1$_V$_1$ is inviscid and the same as the that ($\overline{G}$) in original TGF. When both of temporal and spatial viscous dissipation effects (all order viscosity coefficient terms) are taken into account in $\widetilde{G}_{1\_\infty}$, the instantaneous term $\overline{G}_{1\_\infty}$ for TGF$_1$_V$_\infty$ contains spatial viscous dissipation effects. The newly developed TGF$_1$_V$_\infty$ is shown in Table 1 and compared to the conventional TGF and TGF$_1$_V$_1$.

Table 1. Comparison of newly developed 2D time-domain Green's functions TGF$_1$_V$_\infty$ with TGF$_1$_V$_1$ and conventional Green's functions TGF. The TGF$_1$_V$_n$ ($n = 1, \infty$) are derived from a "fairly perfect fluid" model [1]. In TGF$_1$_V$_1$ only the first order viscous dissipation effects are exactly considered, while in TGF$_1$_V$_\infty$ all order viscous dissipation effects are fully considered. The exact viscous dissipation effects in TGF$_1$_V$_\infty$ appear not only in the free-surface memory term of the Green's function, but also in the instantaneous term. ϵ is the non-dimensional viscosity coefficient, $E_1(\cdot)$ the complex exponential integral function.

2D Time-Domain Green's Function		TGF	TGF$_1$_V$_1$	TGF$_1$_V$_\infty$
Viscous dissipation effects in free-surface memory term	Temporal effect	-	$e^{-\epsilon\omega(t-\tau)}$	$e^{-\epsilon\omega(t-\tau)}$
	Spatial effect	-	-	$e^{\epsilon^2 k_0 R_{p\bar{q}}}$
Instantaneous term		$\ln\frac{r_{pq}}{r_{p\bar{q}}}$	$\ln\frac{r_{pq}}{r_{p\bar{q}}}$	$\mathrm{Re}\{E_1(-\epsilon^2 k_0 R_{p\bar{q}}) - E_1(-\epsilon^2 k_0 R_{pq})\}$

2.3.4. Characteristics of the Instantaneous Term of TGF$_1$_V$_\infty$

To analyze the characteristics of $\overline{G}_{1\_\infty}$, some special cases are discussed as follows. Firstly, considering the case with small value of ϵ, it is well known that the complex exponential integral $E_1(-\epsilon^2 k_0 z)$ can be expanded as the following series

$$E_1\left(-\epsilon^2 k_0 z\right) = -\gamma - \ln\left(-\epsilon^2 k_0\right) - \ln z - \sum_{n=1}^{\infty} \frac{k_0^n z^n}{n!n} \epsilon^{2n} \tag{15}$$

where γ is the Euler constant. The expansion (Equation (15)) holds at $\epsilon \to 0$ and $|z| < 1$. Using Equation (15), the instantaneous terms in Equation (14) can be expanded as

$$\overline{G}_{1\_\infty} = \ln\frac{r_{pq}}{r_{p\bar{q}}} - k_0 \times \mathrm{Re}\{R_{p\bar{q}} - R_{pq}\}\epsilon^2 + O\left(\epsilon^4\right) \tag{16}$$

Equation (16) suggests that when the viscosity coefficients approach zero, the instantaneous term $\overline{G}_{1\_\infty}$ approaches to the inviscid term $\overline{G}$.

Another important characteristic of $\overline{G}_{1\_\infty}$ is its asymptotic behavior. It is known that when $z \to \infty$, the asymptotic expansion of $E_1(z)$ is

$$E_1(z) \sim \frac{e^{-z}}{z}\left(1 - \frac{1!}{z} + \frac{2!}{z^2} - \frac{3!}{z^3} + \cdots\right) \tag{17}$$

If the source point q locates on S_∞, denoting the distance between p and q by $r_\infty = r_{pq} \cong r_{p\bar{q}} \to \infty$, then according to Equation (17), the asymptotic expansion of $\overline{G}_{1\_\infty}(p, q; \epsilon)$ can be written as

$$\overline{G}_{1\_\infty}(p, q; \epsilon)\big|_{q \in S_\infty} \sim O\left(\frac{e^{-\epsilon^2 k_0 r_\infty}}{\epsilon^2 k_0 r_\infty^2}\right) \tag{18}$$

In contrast, the asymptotic expansion of the inviscid instantaneous term $\overline{G}$ is

$$\overline{G}(p, q)\big|_{q \in S_\infty} \sim O\left(\frac{1}{r_\infty}\right) \tag{19}$$

Comparing Equation (18) with Equation (19), one observes that if the viscosity coefficient is sufficient large, the instantaneous term $\overline{G}_{1\_\infty}$ decays with r_{pq} much faster than the inviscid term $\overline{G}$.

2.4. Boundary Integral Equation Using $TGF_{1\_}V_n$

The unknown constant β in Equation (10) is solved in Appendix B, and the final result is $\beta = 1$. Thereby, according to Equation (A6) in Appendix A, we obtain the boundary integral equation

$$
\begin{aligned}
2\pi\psi(t,\boldsymbol{p}) \quad & +\int_{S_{\mathrm{B}}}\left(\overline{G}_{1\_n}\frac{\partial\psi(t,\boldsymbol{q})}{\partial n_q} - \psi(t,\boldsymbol{q})\frac{\partial\overline{G}_{1\_n}}{\partial n_q}\right)\mathrm{d}s_q \\
& = \int_0^t \mathrm{d}\tau \int_{S_{\mathrm{B}}}\left(\widetilde{G}_{1\_n}\frac{\partial\psi(\tau,\boldsymbol{q})}{\partial n_q} - \psi(\tau,\boldsymbol{q})\frac{\partial\widetilde{G}_{1\_n}}{\partial n_q}\right)\mathrm{d}s_q
\end{aligned}
\tag{20}
$$

Equation (20) is a mixed source and dipole distribution model. One might prefer to use the pure source distribution model in numerical practice. Extending the fluid domain into the interior of the floating body, and, respectively, applying Green's theorem to $TGF_{1\_}V_n$ in exterior and interior fluid domain, one gets boundary integral equation only with source points distributing on the mean wetted body surface

$$
2\pi\psi(t,\boldsymbol{p}) + \int_{S_{\mathrm{B}}}\sigma(t,\boldsymbol{q})\overline{G}_{1\_n}\mathrm{d}s_q = \int_0^t \mathrm{d}\tau \int_{S_{\mathrm{B}}}\sigma(\tau,\boldsymbol{q})\widetilde{G}_{1\_n}\mathrm{d}s_q
\tag{21}
$$

where σ is the source density. Taking the derivative of Equation (21) with respect to normal vector $\boldsymbol{n}_p$ on point $\boldsymbol{p}$, the source density equation is obtained

$$
-\pi\sigma(t,\boldsymbol{p}) + \int_{S_{\mathrm{B}}}\sigma(t,\boldsymbol{q})\frac{\partial\overline{G}_{1\_n}}{\partial n_p}\mathrm{d}s_q = -2\pi V_n(t,\boldsymbol{p}) + \int_0^t \mathrm{d}\tau \int_{S_{\mathrm{B}}}\sigma(\tau,\boldsymbol{q})\frac{\partial\widetilde{G}_{1\_n}}{\partial n_p}\mathrm{d}s_q
\tag{22}
$$

where $V_n(t,\boldsymbol{p})$ is the velocity of point $\boldsymbol{p}$ in outward normal direction.

3. Application of $TGF_{1\_}V_\infty$ for Solving Interaction between Water Waves and Floating Bodies with Considering Viscous Dissipation Effects

In Section 2, a novel Green's function $TGF_{1\_}V_\infty$ was developed and here it is utilized to solve two typical interaction problems between water waves and floating bodies that were not well addressed using TGF or TGF_V_1 in literature. The first is a wedge with flare angle of $45°$ heaving on the water surface, which could induce numerical instability when using TGF. The second is a hull section with sharp keel rolling on the water surface, in which significant vortex shedding occurs. For the purpose of comparison, numerical results from TGF and $TGF_{1\_}V_1$ are also provided in the cases.

3.1. Wedge Heaving on the Water Surface

The wedge–water interaction represents a type of common marine engineering hydrodynamic problems, such as ship bow slamming, planing craft navigates on water surface, seaplane lands on water and so on. The wedges generally are not wall-sided, or with flare angle. It is well-known that numerical instability might appear when using TGF to evaluate hydrodynamics of floating bodies with flare angles. Several numerical tricks were proposed to conquer this difficulty. For example, Dai and Duan [10] modified the upper limit of the integral with respect to wave number in the free-surface memory term from infinity to a finite value. Duan [12] set the source density on the segment adjacent to water surface to zero. Beyond that, the numerical instability was considered to have relation with no consideration of the viscous dissipation effects in the flow, so Wu [9] made an attempt to solve it using a viscous correction approach. He exploited a 3D $TGF_{2\_}V_1$ to study a heaving cone, but the numerical instability was not completely eliminated. In this work, a similar problem is to be solved using $TGF_{1\_}V_\infty$.

As shown in Figure 1, we consider a 2D wedge with mean draught $d = 1$ m, half of mean breadth $b = 1$ m, flare angle $\theta = 45°$, which harmonically heaves on the water surface with frequency $\omega = 0.8$ rad/s. The problem is considered in the linear framework, so the heave amplitude is assumed to be unit. Each side of the wetted surface is equally divided into 50 segments, and let $s = 1, 2, \cdots, 50$ be indices of segments orderly from toppest one to the lowest one under water surface. In this case,

the numerical instability rises when using the conventional TGF to solve the hydrodynamic force acting on the wedge. Here the newly developed $TGF_1\_V_\infty$ is employed to improve the numerical stability. In this method, the heave frequency is set as the reference frequency in the viscosity coefficient, and five empirically selected non-dimensional viscosity coefficient values $\epsilon = 12.5, 10, 7.5, 5.0, 2.5$, are respectively imposed onto the field points on the first five segments ($s = 1 \sim 5$) on each side of the wetted surface, while the viscosity coefficients on the rest segments are set to zero. The basic concept of this methodology is to set an artificial thin viscous layer right below the water surface with gradually decreasing viscosity, which is expected to maintain the numerical stability at segments adjacent to water surface, since the divergence always occurs firstly at these segments. Noting that the numerical instability only occurs at the step of solving source density, we reset viscosity coefficient values on all segments to zero once source density has been solved. TGF and $TGF_1\_V_1$ are employed for comparison.

Figure 2 panels (a–f) portray the time series of source density σ_3 (real part and imaginary part) on segments $s = 1, 5, 50$ using methods TGF, $TGF_1\_V_1$ and $TGF_1\_V_\infty$. One can observe that on all segments the source density solved by the inviscid TGF diverges within a few heave periods. Moreover, the closer the segment approaches to free surface, the faster the source density diverges. The method $TGF_1\_V_1$ does not improve the results too much, but exaggerates the amplitude of source density. In contrast, the method $TGF_1\_V_\infty$ desirably smooths the time series of source density without changing amplitudes or phases, and the results show significant periodic characteristics with the same period as heave motion. One can notice that, in Figure 2c,d, oscillations with higher frequency occur in the source density obtained by $TGF_1\_V_\infty$, but they do not bring in numerical instability. In Figure 2a–f, it is also worth noting that the amplitude of source densities gradually decreases from $s = 1$ to $s = 50$, while the phase almost remains the same.

Figure 3a,b depicts the time series of non-dimensional heave force $f_3/\Delta g$ (real part and imaginary part), where Δ is the mean immersed volume of the wedge. The TGF results diverge after two periods, while the $TGF_1\_V_1$ results are slightly better, diverging after four periods. In contrast, the $TGF_1\_V_\infty$ results are very stable in both of instantaneous state and steady state. One can even find that, in the first two periods, the $TGF_1\_V_1$ results detectably deviate from the TGF ones at the crests or troughs, while the $TGF_1\_V_\infty$ results agree well with TGF ones. Moreover, the amplitude of the non-dimensional heave force obtained by $TGF_1\_V_\infty$ in Figure 3a is $|Re\{f_3/\Delta g\}| = 0.291$, while that from an in-house frequency-domain strip method STF is $|Re\{f_3/\Delta g\}| = 0.279$, which further confirms the validity of the $TGF_1\_V_\infty$ method.

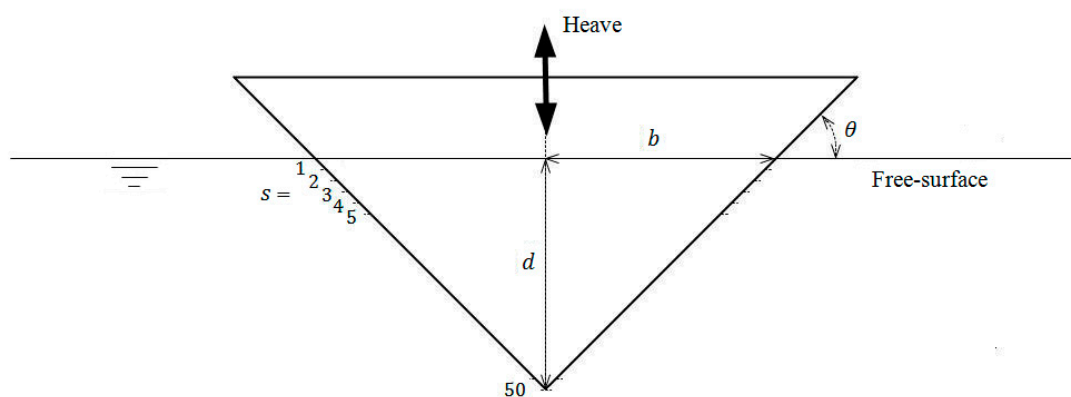**Figure 1.** A wedge harmonically heaves on the water surface, with mean draught $d = 1$ m, half of mean breadth $b = 1$ m, flare angle $\theta = 45°$, and heave frequency $\omega = 0.8$ rad/s. Each side of the wetted surface of the wedge are equally divided into 50 segments.
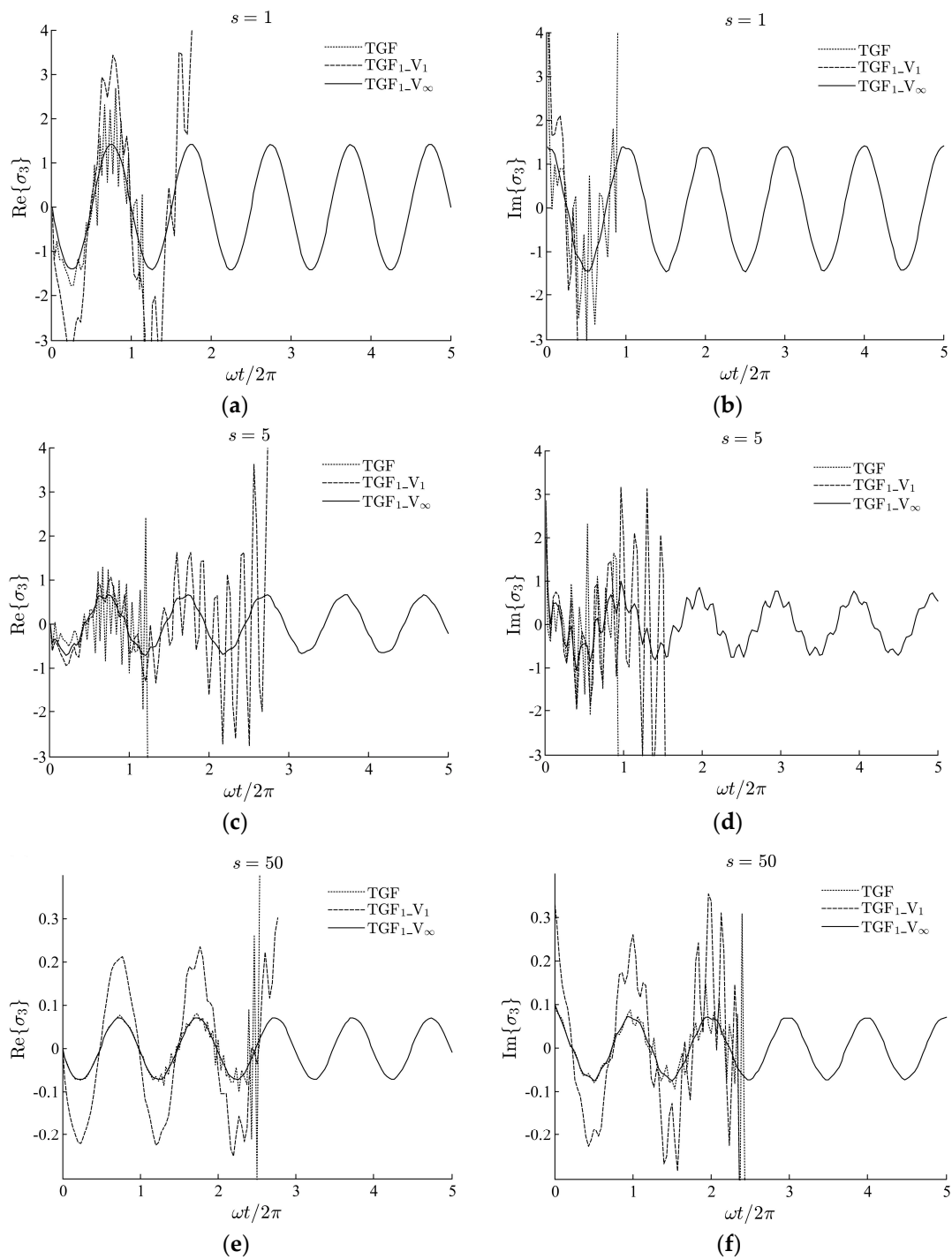
Figure 2. Comparison of time series of source density (real and imaginary part) on segments $s = 1, 5, 50$ using methods TGF, $\text{TGF}_1\_V_1$ and $\text{TGF}_1\_V_\infty$. In $\text{TGF}_1\_V_1$, only the temporal viscous dissipation effects is considered, while in $\text{TGF}_1\_V_\infty$ both temporal and spatial viscous dissipation effects are taken into account. In $\text{TGF}_1\_V_n$, the reference frequency is set as the heave frequency: $\omega_0 = 0.8$ rad/s, five non-dimensional viscosity coefficient values $\epsilon = 12.5,\ 10,\ 7.5,\ 5.0,\ 2.5$ are respectively imposed onto the field points on the first five segments ($s = 1 \sim 5$) on each side of the wetted surface. (**a**) Real part of source density on segment $s = 1$; (**b**) Imaginary part of source density on segment $s = 1$; (**c**) Real part of source density on segment $s = 5$; (**d**) Imaginary part of source density on segment $s = 5$; (**e**) Real part of source density on segment $s = 50$; (**f**) Imaginary part of source density on segment $s = 50$.
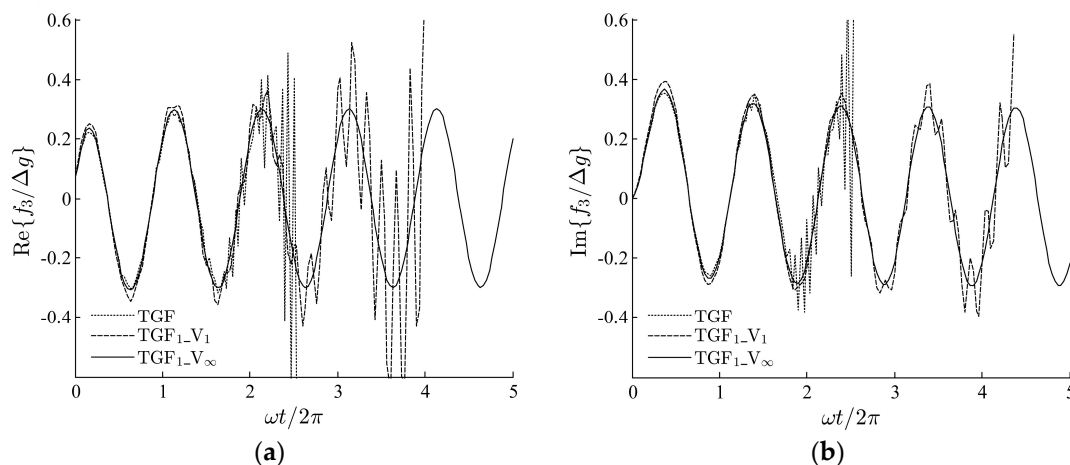
Figure 3. Comparison of time series of heave forces (real and imaginary part) using methods TGF, $TGF_1\_V_1$ and $TGF_1\_V_\infty$. The viscous dissipation effects in $TGF_1\_V_n$ are considered only at the step of solving source density, after which the viscosity coefficient on all segments is set to zero. (**a**) Real part of heave force; (**b**) Imaginary part of heave force.

The numerical results in this case confirm the possibility of improving the numerical stability of the TGF method on solving oscillating floating bodies with flare angle using $TGF_1\_V_\infty$, in which the viscosity coefficient on the flow field near water surface is deliberately enlarged. In contrast, in Wu [9], the viscosity coefficient in $TGF_2\_V_1$ was setting as the physical viscosity of water, which is not strong enough to improve the numerical stability of the TGF method. Moreover, the failure of $TGF_1\_V_1$ in this case suggests that the spatial viscous dissipation effects (higher order viscosity coefficient), which was never considered in literature, should not be ignored when the viscosity coefficient is deliberately heightened.

3.2. Hull Section with Sharp Keel Rolling on the Water Surface

In contrast to the success on evaluating heave and pitch motions of ship hulls in waves using inviscid potential theories, it is difficult to accurately predict the roll of hulls with bilges or sharp edges due to the lack of viscous damping in those methods, even if the motion amplitude is small. To improve the numerical results, empirical corrections were added to the classical strip-theory [13], 2.5D method [14] or 3D Rankine panel methods [15], even vortex shedding methods were embedded into potential flows [16]. Chen et al. [7] and Cummins and Dias [8] employed frequency-domain $GF_1\_V_1$ combined with pressure discharge methods to simulate the energy loss around sharp edges of floating bodies, in which a dissipation surface was added or specified near the sharp edge, and a continuous flow velocity but a discontinuous pressure were imposed across the surface. In this work, we attempt to evaluate hydrodynamics of a hull section with sharp keel rolling on water surface straightforwardly using the newly developed $TGF_1\_V_\infty$ without any pressure discharge methods.

As shown in Figure 4, we consider a hull section S22 with sharp keel investigated in [17], which has mean draught $d = 9.5$ m and half of mean breadth $b = 4.5$ m. The hull section harmonically rolls on the water surface with frequencies $\omega = 0.4 \sim 2.6$ rad/s, which covers nearly all possible frequencies encountered in real sea waves. In the linear framework, the roll amplitude is assumed to be unit. Each side of the wetted surface is equally divided into 60 segments, and let $s = 1, 2, \cdots, 60$ be indices of segments orderly from top most one to the bottom most one under water surface.
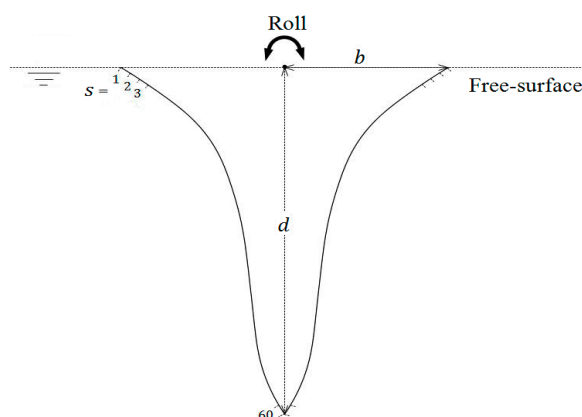
Figure 4. A hull section S22 with sharp keel [17] harmonically rolls on the water surface, with mean draught $d = 9.5$ m, half of mean breadth $b = 4.5$ m, roll frequencies $\omega = 0.4 \sim 2.6$ rad/s. Each side of the wetted surface is equally divided into 60 segments.

Noting that the section S22 has flare angle, we need to eliminate the numerical instability of the TGF method. One could employ the approach proposed in the last sub-Section to do so. However, the distribution of viscosity coefficient values in the flow field for eliminating the numerical instability might not satisfy the requirement for capturing the viscous dissipation effects in rolls. Therefore, in this case we adopt another approach, e.g., setting the source density on the segments adjacent to water surface at each time step to zero [12], to eliminate the numerical instability. After several tries, we set the source density on the first 3 segments ($s = 1 \sim 3$) of each side adjacent to water surface to zero, under the condition of which the numerical stability holds when using $TGF_1\_V_\infty$ to study rolls of the section S22.

Here we take the roll frequency as the reference frequency in the viscosity coefficient, and set the non-dimensional viscosity coefficient as $\epsilon = 0.15$ for the whole flow field, which can lead to pretty good results. The viscous dissipation effects generated by this viscosity coefficient are supposed to capture the pressure loss in the vicinity of sharp keel.

Figure 5a,b depicts the roll-into-roll added mass and damping coefficients, respectively. Figure 5c,d depicts the roll-into-sway added mass and damping coefficients, respectively. The CFD results were obtained in [17] using solver OpenFOAM, in which the roll amplitude is fixed at $3.21°$ and significant vortex shedding phenomenon was observed. As suggested by Lavrov et al. [17], the hydrodynamic coefficients from TGF, $TGF_1\_V_1$ and $TGF_1\_V_\infty$ are calculated using cosine and sine Fourier transforms of the force or moment at a steady phase.

In Figure 5, one can observe that there exists significant discrepancy between inviscid TGF and CFD results, while the $TGF_1\_V_\infty$ results agree well with the CFD ones. In fact, $TGF_1\_V_\infty$ not only accurately predicts the roll damping by taking viscous damping that is ignored by TGF into account, but also significantly improves the added mass of the roll section S22. This result suggests that the viscous dissipation effects have an impact not only on the roll damping, but also on the added mass, though the viscous damping might dominate the influence of viscosity.

On the other hand, it is obvious that the agreement between $TGF_1\_V_1$ and CFD results is not as well as that between $TGF_1\_V_\infty$ and CFD results, especially the added mass in Figure 5a,c. This suggests that the spatial viscous dissipation effects (higher order viscosity coefficient) also play an important role in the whole viscous dissipation effects, which should not be ignored when the viscosity coefficient is sufficient large in the vortex shedding cases.

Admittedly, the $TGF_1\_V_\infty$ does not perform well at low frequencies, which might due to underestimating viscosity coefficient when setting $\epsilon = 0.15$ in this frequency region. To make $TGF_1\_V_\infty$ work better, more samples are needed for training to summarize a more practical viscosity coefficient value.
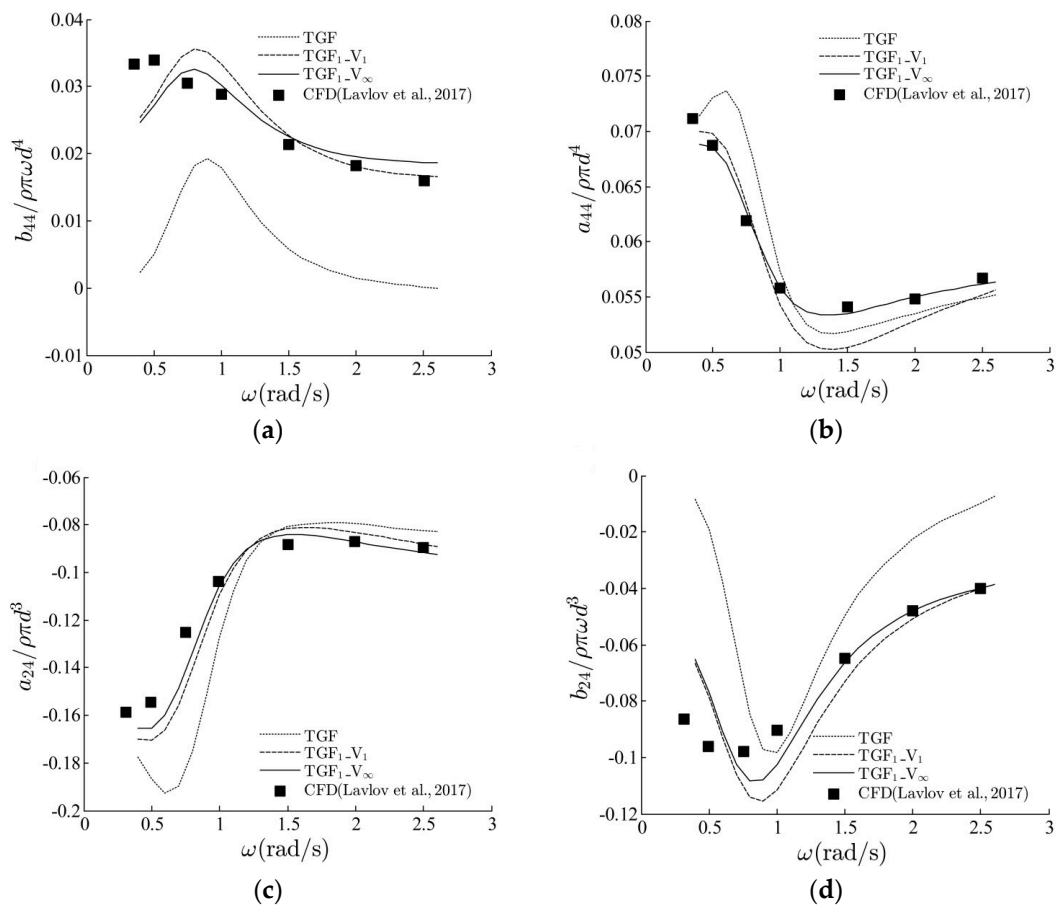
Figure 5. Hydrodynamic coefficients of section S22 using TGF, $TGF_1\_V_1$ and $TGF_1\_V_\infty$ are compared with CFD results [17]. The non-dimensional viscosity coefficient in $TGF_1\_V_1$ and $TGF_1\_V_\infty$ is set as $\epsilon = 0.15$ on all segments and the roll of frequency ω is set as the reference frequency in viscosity coefficient: (**a**) roll-into-roll added mass coefficients; (**b**) roll-into-roll damping coefficients; (**c**) roll-into-sway added mass coefficients; and (**d**) roll-into-sway damping coefficients.

The numerical results in this case suggest that the $TGF_1\_V_\infty$ can be directly employed for capturing the pressure loss of a floating body rolling on the water surface with vortex shedding in the vicinity of the sharp edge. In contrast, in works of Chen et al. [7] or Cummins and Dias [8], the $GF_1\_V_1$ mainly relies on an additional pressure discharge model to capture the pressure loss. The $TGF_1\_V_1$ results in this case also points out the importance of spatial viscous dissipation effects (second order viscosity coefficient), which can significantly improve the hydrodynamic coefficients with viscous dissipation effects. Moreover, as compared to those viscous damping correction methods [13,15] that only make corrections on the damping coefficient, the $TGF_1\_V_\infty$ can consider the viscous dissipation effects not only on damping coefficient, but also on added mass coefficient.

4. Conclusions

This paper presents a novel time-domain Green's function ($TGF_1\_V_\infty$) for the 2D interaction between water waves and floating bodies with viscous dissipation effects. The $TGF_1\_V_\infty$ is derived through the definite problem based on "fairly perfect fluid". The newly proposed $TGF_1\_V_\infty$ is different from the existing ones (TGF_V_1) as follows. In $TGF_1\_V_\infty$, both the temporal (lower order viscosity coefficient term) and spatial (higher order viscosity coefficient term) viscous dissipation effects are taken into account, while the existing TGF_V_1 can only consider the temporal viscous dissipation effects. In $TGF_1\_V_\infty$, both the free-surface memory term and instantaneous term contain

viscous dissipation effects, while, in the existing TGF_V_1, only the free-surface memory term has viscous dissipation effects.

The advantages of TGF$_1$_V$_\infty$ are demonstrated through two typical cases. One is a wedge with flare angle heaving on the water surface. The numerical results suggest that the method based on TGF$_1$_V$_\infty$ gives stable numerical results while these from the method based on the existing Green's function (TGF$_1$_V$_1$) lead to divergent and/or unstable results. The results indicate that the spatial viscous dissipation effects play an important role in eliminating the numerical instability associated with the existing methods. The other case is a hull section of a ship with a sharp keel rolling on the water surface, in which vortex shedding phenomenon appears. The comparison of the results from the methods based on TGF$_1$_V$_\infty$ and the existing Green's function with these results from CFD simulations suggests that the viscous dissipation effects have impact not only on the roll damping, but also on the roll added mass, and that the method based on the new TGF$_1$_V$_\infty$ can give much closer results to the CFD simulations.

Moreover, the newly developed instantaneous term in the TGF$_1$_V$_\infty$ has an advantage of faster decay rate than that of the existing Green's function when the distance between the field and source points increases, which can significantly reduce the computational costs when employing it as the Green's function of Rankine panel methods.

In the future, the time-domain Green's functions (TGF$_1$_V$_\infty$) for the 3D interaction between water waves and floating bodies with viscous dissipation effects will be developed to be able to solve more practical problems.

Author Contributions: Zhiqun Guo and Q. W. Ma developed the time-domain Green's function; Hongde Qin performed the numerical calculations; and Zhiqun Guo wrote the paper.

Appendix A

Let S_F, S_B, S_∞ be the water surface, wetted surface of floating body, and surrounding surface at infinity, respectively. The velocity potential at point q at time τ is denoted by $\psi(\tau, q)$. Applying Green's theorem to $\psi(\tau, q)$ and $G_{1\_n}(p, t; q, \tau; \epsilon)$, one obtains

$$\int_0^t d\tau \int_{S_F + S_B + S_\infty} \left(\psi(\tau, q) \frac{\partial G_{1\_n}}{\partial n_q} - G_{1\_n} \frac{\partial \psi(\tau, q)}{\partial n_q} \right) ds_q = 2\pi \beta \psi(t, q) \tag{A1}$$

where β is an unknown constant decided by the instantaneous term in G_{1_n}.

The free-surface term $\widetilde{G}_{1\_n}$ is harmonic in the fluid domain, so applying Green's theorem to $\psi(\tau, q)$ and $\widetilde{G}_{1\_n}$, we have

$$\int_0^t d\tau \int_{S_F + S_B + S_\infty} \left(\psi(\tau, q) \frac{\partial \widetilde{G}_{1\_n}}{\partial n_q} - \widetilde{G}_{1\_n} \frac{\partial \psi(\tau, q)}{\partial n_q} \right) ds_q = 0 \tag{A2}$$

Using the boundary conditions for $\widetilde{G}_{1\_n}$ on S_∞, it can be deduced that the integral of Equation (A2) on S_∞ equals to 0. Using the initial and free-surface conditions for $\psi(\tau, q)$ and first kind $\widetilde{G}_{1\_n}(p, t; q, \tau; \epsilon)$, the integral (A2) on S_F can be transformed to

$$
\begin{aligned}
\int_0^t d\tau \int_{S_F} \left(\psi \frac{\partial \widetilde{G}_{1\_n}}{\partial n_q} - \widetilde{G}_{1\_n} \psi_{n_q} \right) ds_q
&= -\frac{1}{g} \int_0^t d\tau \int_{S_F} \left(\psi \left(\frac{\partial^2 \widetilde{G}_{1\_n}}{\partial \tau \partial \tau} - 2\epsilon\omega \frac{\partial \widetilde{G}_{1\_n}}{\partial \tau} \right) - \widetilde{G}_{1\_n} (\psi_{\tau\tau} + 2\epsilon\omega\psi_\tau) \right) ds_q \\
&= -\frac{1}{g} \int_{S_F} \left(\psi \frac{\partial \widetilde{G}_{1\_n}}{\partial \tau} - \widetilde{G}_{1\_n}\psi_\tau - 2\epsilon\omega\psi\widetilde{G}_{1\_n} \right) \big|_{\tau=0}^t ds_q \\
&= -\frac{1}{g} \int_{S_F} \psi \frac{\partial \widetilde{G}_{1\_n}}{\partial \tau} \big|_{\tau=0}^t ds_q
\end{aligned} \tag{A3}
$$

Substituting Equation (A3) into Equation (A2) yields

$$
\int_0^t d\tau \int_{S_B} \left(\psi(\tau, \boldsymbol{q}) \frac{\partial \widetilde{G}_{1\_n}}{\partial n_q} - \widetilde{G}_{1\_n} \frac{\partial \psi(\tau, \boldsymbol{q})}{\partial n_q} \right) ds_q = \frac{1}{g} \int_{S_F} \psi(\tau, \boldsymbol{q}) \frac{\partial \widetilde{G}_{1\_n}}{\partial \tau} \bigg|_{\tau=t} ds_q \tag{A4}
$$

On the other hand, substituting Equation (A2) into Equation (A1), and taking Equation (3) into account, one obtains

$$
\int_0^t d\tau \int_{S_F+S_B+S_\infty} \left(\psi(\tau, \boldsymbol{q}) \frac{\partial \left(\delta(t-\tau)\overline{G}_{1\_n} \right)}{\partial n_q} - \delta(t-\tau)\overline{G}_{1\_n} \frac{\partial \psi(\tau, \boldsymbol{q})}{\partial n_q} \right) ds_q = 2\pi\beta\psi(t, \boldsymbol{q})
$$

i.e.,

$$
\int_{S_F+S_B+S_\infty} \left(\psi(t, \boldsymbol{q}) \frac{\partial \overline{G}_{1\_n}}{\partial n_q} - \overline{G}_{1\_n} \frac{\partial \psi(t, \boldsymbol{q})}{\partial n_q} \right) ds_q = 2\pi\beta\psi(t, \boldsymbol{q})
$$

or

$$
\begin{aligned}
&\int_{S_B} \left(\psi(t, \boldsymbol{q}) \frac{\partial \overline{G}_{1\_n}}{\partial n_q} - \overline{G}_{1\_n} \frac{\partial \psi(t, \boldsymbol{q})}{\partial n_q} \right) ds_q - 2\pi\beta\psi(t, \boldsymbol{q}) \\
&= \int_{S_F+S_\infty} \left(\overline{G}_{1\_n} \frac{\partial \psi(t, \boldsymbol{q})}{\partial n_q} - \psi(t, \boldsymbol{q}) \frac{\partial \overline{G}_{1\_n}}{\partial n_q} \right) ds_q
\end{aligned} \tag{A5}
$$

Subtracting Equation (A4) from Equation (A5) yields

$$
\begin{aligned}
&\int_{S_B} \left(\psi \frac{\partial \overline{G}_{1\_n}}{\partial n_q} - \overline{G}_{1\_n} \frac{\partial \psi}{\partial n_q} \right) ds_q - \int_0^t d\tau \int_{S_B} \left(\psi \frac{\partial \widetilde{G}_{1\_n}}{\partial n_q} - \widetilde{G}_{1\_n} \frac{\partial \psi}{\partial n_q} \right) ds_q - 2\pi\beta\psi \\
&= \int_{S_F} \overline{G}_{1\_n} \frac{\partial \psi}{\partial \eta} ds_q - \int_{S_F} \psi \left(\frac{\partial \overline{G}_{1\_n}}{\partial n_q} + \frac{1}{g} \frac{\partial \widetilde{G}_{1\_n}}{\partial \tau} \bigg|_{\tau=t} \right) ds_q \\
&\quad - \int_{S_\infty} \left(\psi \frac{\partial \overline{G}_{1\_n}}{\partial n_q} - \overline{G}_{1\_n} \frac{\partial \psi}{\partial n_q} \right) ds_q
\end{aligned} \tag{A6}
$$

If the right hand side of Equation (A6) equals to 0, i.e., $\overline{G}_{1\_n} = \frac{\partial \overline{G}_{1\_n}}{\partial n_q} + \frac{1}{g} \frac{\partial \widetilde{G}_{1\_n}}{\partial \tau} \big|_{\tau=t} = 0$ on S_F, and $\overline{G}_{1\_n} \sim O(1/r_{pq})$ on S_∞, the singular points can be distributed only on the wetted surface S_B. Therefore, the definite conditions for the instantaneous term $\overline{G}_{1\_n}(\boldsymbol{p}, \boldsymbol{q}; \epsilon)$ can be concluded as following

$$
\begin{cases}
\nabla_q^2 \overline{G}_{1\_n} = \beta\delta(\boldsymbol{p} - \boldsymbol{q}), & \boldsymbol{p}, \boldsymbol{q} \in \Omega \\
\overline{G}_{1\_n} = 0, & \eta = 0 \\
\overline{G}_{1\_n} \sim O\left(\frac{1}{r_{pq}} \right), & r_{pq} \to \infty \\
\frac{\partial \overline{G}_{1\_n}}{\partial \eta} = -\frac{1}{g} \frac{\partial \widetilde{G}_{1\_n}}{\partial \tau}, & t = \tau, \eta = 0
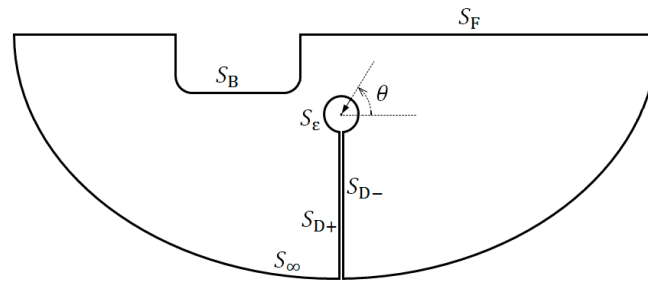\end{cases} \tag{A7}
$$

Appendix B

Figure A1. The integral path for the instantaneous term $\overline{G}_{1\_\infty}(p, q; \epsilon)$.

The harmonic characteristic of $\overline{G}_{1\_\infty}(p, q; \epsilon)$ ($p \neq q$) can be easily verified. Thereby, applying Green's theorem to $\psi(t, q)$ and $\overline{G}_{1\_\infty}(p, q; \epsilon)$ yields

$$\int_{S_F+S_B+S_\infty+S_\varepsilon+S_{D+}+S_{D-}} \left(\psi \frac{\partial \overline{G}_{1\_\infty}}{\partial n_q} - \overline{G}_{1\_\infty} \frac{\partial \psi}{\partial n_q} \right) ds_q = 0 \tag{A8}$$

Since the point $\overline{q}$ locates at the upper half space, the Green's theorem with respect to $\psi(t, q)$ and $\text{Re}\{E_1(-\epsilon^2 k_0 R_{p\overline{q}})\}$ equals to 0 and the integral of Equation (A8) on $S_\varepsilon + S_{D+} + S_{D-}$ reduces to

$$\begin{aligned} &\int_{S_\varepsilon+S_{D+}+S_{D-}} \left(\psi \frac{\partial \overline{G}_{1\_\infty}}{\partial n_q} - \overline{G}_{1\_\infty} \frac{\partial \psi}{\partial n_q} \right) ds_q \\ = \ &\int_{S_\varepsilon+S_{D+}+S_{D-}} \left(\text{Re}\{E_1(-\epsilon^2 k_0 R_{pq})\} \frac{\partial \psi}{\partial n_q} - \psi \frac{\partial \text{Re}\{E_1(-\epsilon^2 k_0 R_{pq})\}}{\partial n_q} \right) ds_q \end{aligned} \tag{A9}$$

Defining $r_\varepsilon = |R_{pq}|$, according to Equation (15), the first term at right hand side of Equation (A9) on S_ε can be expanded as

$$\begin{aligned} &\int_{S_\varepsilon} \text{Re}\{E_1(-\epsilon^2 k_0 R_{pq})\} \frac{\partial \psi}{\partial n_q} ds_q \\ = \ &\int_{S_\varepsilon} \frac{\partial \psi}{\partial n_q} \left(-\gamma - \ln|\epsilon^2 k_0 R_{pq}| + O(r_\varepsilon) \right) ds_q \\ \overset{r_\varepsilon \to 0}{=} \ &\frac{\partial \psi(t,p)}{\partial n_q} \int_0^{2\pi} \left(-\gamma - \ln(\epsilon^2 k_0 r_\varepsilon) \right) r_\varepsilon d\theta = 0 \end{aligned} \tag{A10}$$

As shown in Figure A1, the second term at right hand side of Equation (A9) on S_ε can be calculated as follows

$$\begin{aligned} &\int_{S_\varepsilon} \psi \frac{\partial \text{Re}\{E_1(-\epsilon^2 k_0 R_{pq})\}}{\partial n_q} ds_q \\ = \ &\int_0^\pi \psi \text{Re}\left\{ \exp\left(\epsilon^2 k_0 r_\varepsilon e^{i(\frac{3\pi}{2}-\theta)} \right) \right\} d\theta \\ + \ &\int_\pi^{2\pi} \psi \text{Re}\left\{ \exp\left(\epsilon^2 k_0 r_\varepsilon e^{i(\theta-\frac{\pi}{2})} \right) \right\} d\theta \overset{r_\varepsilon \to 0}{=} 2\pi\psi \end{aligned} \tag{A11}$$

The integral at right hand side of Equation (A9) on $S_{D+} + S_{D-}$ equals to 0 due to the inverse gradient direction on S_{D-} and S_{D+}, i.e.,

$$\int_{S_{D+}+S_{D-}} \left(\text{Re}\{E_1(-\epsilon^2 k_0 R_{pq})\} \frac{\partial \psi}{\partial n_q} - \psi \frac{\partial \text{Re}\{E_1(-\epsilon^2 k_0 R_{pq})\}}{\partial n_q} \right) ds_q = 0 \tag{A12}$$

Combining Equations (A8)–(A12) yields

$$\int_{S_F+S_B+S_\infty} \left(\psi \frac{\partial \overline{G}_{1\_\infty}}{\partial n_q} - \overline{G}_{1\_\infty} \frac{\partial \psi}{\partial n_q} \right) ds_q = 2\pi\psi \tag{A13}$$

Therefore, the unknown constant β in Equations (10) and (A7) equals to

$$\beta = 1 \qquad\qquad\qquad (A14)$$

References

1. Guével, P. *Le Problème de Diffraction-Radiation—Première Partie: Théorèmes Fondamentaux*; ENSM, Univ. Nantes: Nantes, France, 1982. (In French)
2. Chen, X.B. Hydrodynamics in offshore and naval applications-Part. In Proceedings of the 6th International Conference on Hydrodynamics, Perth, Australia, 24–26 November 2004.
3. Dias, F.; Dyachenko, A.I.; Zakharov, V.E. Theory of weakly damped free-surface flows: A new formulation based on potential flow solutions. *Phys. Lett. A* **2007**, *372*, 1297–1302. [CrossRef]
4. Chen, X.B.; Dias, F. Visco-potential flow and time-harmonic ship waves. In Proceedings of the 25th International Workshop on Water Waves and Floating Bodies (IWWWFB), Harbin, China, 9–12 May 2010.
5. Yao, C.B.; Dong, W.C. Modeling of fluid resonance in-between two floating structures in close proximity. *J. Zhejiang Univ. Sci. A (Appl. Phys. Eng.)* **2015**, *16*, 987–1000. [CrossRef]
6. Qin, H.D.; Shen, J.; Chen, X.B. A free surface frequency domain Green function with viscous dissipation and partial reflections from side walls. *J. Mar. Sci. Appl.* **2011**, *10*, 259–264. [CrossRef]
7. Chen, X.B.; Dias, F.; Duan, W.Y. Introduction of dissipation in potential flows. In Proceedings of the 7th International Workshop on Ship Hydrodynamics, Shanghai, China, 16–19 September 2011.
8. Cummins, C.P.; Dias, F. A new model of viscous dissipation for an oscillating wave surge converter. *J. Eng. Math.* **2017**, *103*, 195–216. [CrossRef]
9. Wu, G. The Time-Domain Green Function Method Involving Fluid Viscosity. Master's Thesis, Harbin Engineering University, Harbin, China, 2007.
10. Dai, Y.S.; Duan, W.Y. *Potential Flow Theory of Ship Motions in Waves*, 1st ed.; The National Defense Industries Press: Beijing, China, 2008; pp. 253–254. ISBN 9787118053159.
11. Faltinsen, O.; Zhao, R. Numerical predictions of ship motions at high forward speed. *Philos. Trans. R. Soc. B* **1991**, *334*, 241–252. [CrossRef]
12. Duan, W.Y. Nonlinear Hydrodynamic Forces Acting on a Ship Undergoing Large Amplitude Motions. Ph.D. Thesis, Harbin Engineering University, Harbin, China, 1995.
13. Katayama, T.; Yoshioka, Y.; Kakinoki, T.; Ikeda, Y. Some topics for estimation of bilge-keel component of roll damping. In Proceedings of the 11th International Ship Stability Workshop, Wageningen, The Netherlands, 21–23 June 2010; pp. 225–230.
14. Zhang, H.; Li, J.D. Improving longitudinal motion prediction of hybrid monohulls with the viscous effect. *J. Mar. Sci. Appl.* **2007**, *6*, 39–45. [CrossRef]
15. Yasukawa, H. Application of a 3-D time domain panel method to ship seakeeping problems. In Proceedings of the 24th Symposium on Naval Hydrodynamics, Fukuoka, Japan, 8–13 July 2002; pp. 376–392.
16. Downie, M.J.; Dearman, P.W.; Graham, J.M.R. Effect of vortex shedding on the coupled roll response of bodies in waves. *J. Fluid Mech.* **1988**, *189*, 243–261. [CrossRef]
17. Lavrov, A.; Rodrigues, J.M.; Gadelho, J.; Guedes Soares, C. Calculation of hydrodynamic coefficients of ship sections in roll motion using Navier-Stokes equations. *Ocean Eng.* **2017**, *133*, 36–46. [CrossRef]